Epitaxial Growth of Highly Luminescent CdSe/CdS Core/Shell Nanocrystals with Photostability and Electronic Accessibility

Xiaogang Peng, Michael C. Schlamp, Andreas V. Kadavanich, and A. P. Alivisatos*

Contribution from the Department of Chemistry, University of California, Berkeley, and Molecular Design Institute, Lawrence Berkeley Laboratory, Berkeley, California 94720

Received March 10, 1997[⊗]

Abstract: The synthesis of epitaxially grown, wurtzite CdSe/CdS core/shell nanocrystals is reported. Shells of up to three monolayers in thickness were grown on cores ranging in diameter from 23 to 39 Å. Shell growth was controllable to within a tenth of a monolayer and was consistently accompanied by a red shift of the absorption spectrum, an increase of the room temperature photoluminescence quantum yield (up to at least 50%), and an increase in the photostability. Shell growth was shown to be uniform and epitaxial by the use of X-ray photoelectron spectroscopy (XPS), X-ray diffraction (XRD), high resolution transmission electron microscopy (HRTEM), and optical spectroscopy. The experimental results indicate that in the excited state the hole is confined to the core and the electron is delocalized throughout the entire structure. The photostability can be explained by the confinement of the hole, while the delocalization of the electron results in a degree of electronic accessibility that makes these nanocrystals attractive for use in optoelectronic devices.

Introduction

During the past decade, tremendous advances in colloid chemistry have led to the preparation of high quality nanometer sized semiconductor crystals.[1−9] A current challenge is to apply the full range of techniques employed in two-dimensional (2D) artificial structure growth, such as epitaxial growth and band gap patterning,[10,11] to nanocrystals fabricated by wet chemical routes. This paper details the synthesis of an epitaxial core/shell system. In 2D systems, it is possible to prepare either a type I structure, in which both electrons and holes are in their lowest energy states in the same material, or a type II structure, in which their lowest energy states are spatially separated in different materials. In certain 2D structures[12,13] this CdSe/CdS system has yielded a type II quantum well. However, because the kinetic energy of electrons and holes are relatively large in 0D structures,[14] the potential energy steps created by alternating materials in 2D may not always be sufficient to confine carriers in 0D. Such an example is presented here, where the hole is largely confined to the core and the electron is delocalized throughout the core/shell structure.

Because the surface of a nanocrystal is made up of atoms that are not fully coordinated, it is highly active and invites the possibility of epitaxial overgrowth of another semiconductor or other inorganic material. In addition, surface atoms act like defects unless passivated.[15] To remove these defects, high quality homogeneous II−VI and III−V nanocrystals have been passivated with long chain organic surfactants. These "capped" nanocrystals have room temperature photoluminescence quantum yields as high as 10% with a very long fluorescence lifetime and often have some non-band-edge luminescence.[16,17] However, it is generally very difficult to simultaneously passivate both anionic and cationic surface sites by organic ligands; there are always some dangling bonds on the surface. For nanocrystals, inorganic epitaxial growth can not only eliminate both the anionic and cationic surface dangling bonds but also generate a new nanocrystal system with novel properties. Most of the properties of these "core/shell" systems are dependent on both core and shell materials.

Inorganic passivation has been explored in such core/shell systems as Si/SiO_2,[18] $CdS/Cd(OH)_2$,[15] CdSe/ZnSe,[19,20] CdSe/ZnS,[21,22] CdS/HgS/CdS,[23,24] and CdSe/CdS[25] and has been shown to improve luminescence quantum yields,[15,19−23] decrease fluorescence lifetimes,[21] and have other benefits[26] related to the tailoring of relative bandgap positions between the two materials.

[⊗] Abstract published in *Advance ACS Abstracts,* July 1, 1997.

(1) Henglein, A. *Top. Curr. Chem.* **1988**, *143*, 113.
(2) Bawendi, M. G.; Steigerwald, M. L.; Brus, L. E. *Annu. Rev. Phys. Chem.* **1990**, *41*, 477.
(3) Brus, L. E. *Appl. Phys. A* **1991**, *53*, 465.
(4) Wang, Y.; Herron, N. *J. Phys. Chem.* **1991**, *95*, 525.
(5) Heath, J. R. *Science* **1992**, *258*, 1131−1133.
(6) Weller, H. *Adv. Mater.* **1993**, *5*, 88.
(7) Micic, O. I.; Curtis, C. J.; Jones, K. M.; Sprague, J. R.; Nozik, A. J. *J. Phys. Chem.* **1994**, *98*, 4966−4969.
(8) Alivisatos, A. P. *J. Phys. Chem.* **1996**, *100*, 13226.
(9) Alivisatos, A. P. *Science* **1996**, *271*, 933.
(10) Tsu, R.; Esaki, L. *App. Phys. Lett.* **1973**, *22*, 562−564.
(11) Sze, S. M. *Physics of Semiconductor Devices*; Wiley-Interscience: New York, 1986.
(12) Langbein, W.; Hetterich, M.; Grun, M.; Klingshirn, C.; Kalt, H. *Appl. Phys. Lett.* **1994**, *65*, 2466.
(13) Halsall, M. P.; Nicholls, J. E.; Davies, J. J.; Cockayne, B.; Wright, P. J.; Cullis, A. G. *Semicond. Sci. Technol.* **1988**, *3*, 1126.
(14) Rosetti, R.; Nakahara, S.; Brus, L. E. *J. Chem. Phys.* **1983**, *79*, 1086.
(15) Spanhel, L.; Haase, M.; Weller, H.; Henglein, A. *J. Am. Chem. Soc.* **1987**, *109*, 5649.
(16) Norris, D. J.; Sacra, A.; Murray, C. B.; Bawendi, M. G. *Phys. Rev. Lett.* **1994**, *72*, 2612.
(17) Hoheisel, W.; Colvin, V. L.; Johnson, C. S.; Alivisatos, A. P. *J. Chem. Phys.* **1994**, *101*, 8455.
(18) Wilson, W. L.; Szajowski, P. F.; Brus, L. E. *Science* **1993**, *262*, 1242−1244.
(19) Danek, M.; Jensen, K. F.; Murray, C. B.; Bawendi, M. G. *Chem. Mater.* **1996**, *8*, 173.
(20) Hoener, C. F.; Allan, K. A.; Bard, A. J.; Campion, A.; Fox, M. A.; Mallouk, T. E.; Webber, S. E.; White, J. M. *J. Phys. Chem.* **1992**, *96*, 3812.
(21) Hines, M. A.; Guyot-Sionnest, P. *J. Phys. Chem.* **1996**, *100*, 468.
(22) Kortan, A. R.; Hull, R.; Opila, R. L.; Bawendi, M. G.; Steigerwald, M. L.; Carroll, P. J.; Brus, L. E. *J. Am. Chem. Soc.* **1990**, *112*, 1327.
(23) Mews, A.; Eychmuller, A.; Giersig, M.; Schooss, D.; Weller, H. *J. Phys. Chem.* **1994**, *98*, 934.
(24) Mews, A.; Kadavanich, A. V.; Banin, U.; Alivisatos, A. P. *Phys. Rev. B.* **1996**, *53*, 13242.
(25) Tian, Y.; Newton, T.; Kotov, N. A.; Guldi, D. M.; Fendler, J. H. *J. Phys. Chem.* **1996**, *100*, 8927.
(26) Danek, M.; Jensen, K. F.; Murray, C. B.; Bawendi, M. G. *Appl. Phys. Lett.* **1994**, *65*, 2795.

S0002-7863(97)00754-3 CCC: $14.00

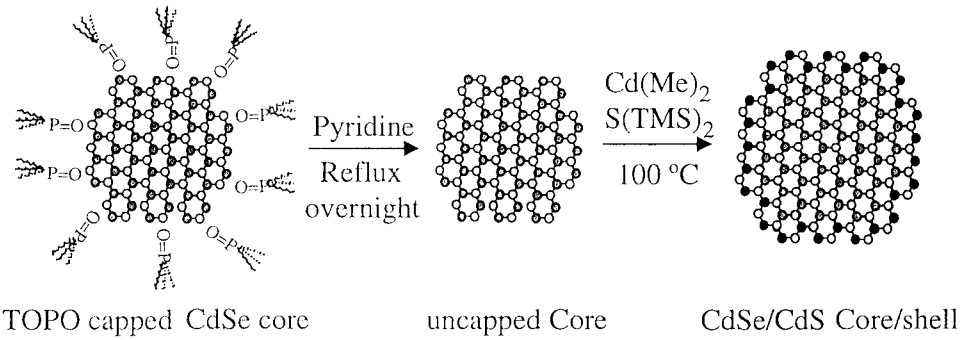

Figure 1. Schematic synthesis of CdSe/CdS core/shell nanocrystals.

Often these efforts have been hindered by a lack of size control or amorphous or nonepitaxial growth.

Reported here is a synthesis of wurtzite CdSe/CdS core/shell nanocrystals. A shell having uniform thickness is grown epitaxially on the core, and the resulting nanocrystals have high room temperature quantum yields (>50%). The wide range of core and shell sizes studied provide tunability of band edge luminescence at these high quantum yields. In this system, the holes are confined to the core, while the electrons are delocalized as a result of the similar electron affinities of the core and shell. As a consequence, the nanocrystals are extremely stable with respect to photooxidation, which requires a hole trapped at the surface. The increase in photochemical stability does not come at the expense of electrical access; electrons are fully delocalized and may be accessed for applications where the ability of a dense matrix of these nanocrystals to both conduct an electron current and luminesce is paramount.

The wurtzite CdSe/CdS system is ideal in many respects. The lattice mismatch of 3.9% is small enough to allow epitaxial growth while still preventing alloying, and the difference in band gaps is large enough for shell growth to increase the quantum yield and stability of the cores. Some of these characteristics of CdSe/CdS epitaxial systems have been observed in 2D superlattices.[13,27−29] During the past several years, the synthesis of CdSe nanocrystals has become well established.[30,31] Monodisperse, faceted, and highly crystalline CdSe nanocrystals can now be reproducibly and controllably synthesized on a gram scale. A high quality core is very helpful for the growth and characterization of the core/shell structures as shown below.

The synthetic conditions presented here allow shells to be grown of varying thicknesses on varying core sizes. The conditions also prevent core dissolution and CdS-only nanocrystal formation during shell growth. The chemistry of shell growth is clean—the added reagents react quantitatively. The resulting reaction provides an additional means for tuning the band gap of the nanocrystals while yielding a stable product which can be treated as a chemical reagent for building up more complex structures.

Experimental Section

(A) Synthesis of Nearly Monodisperse CdSe and CdS Nanocrystals. Chemicals. The dimethylcadmium ($Cd(CH_3)_2$) and tributylphosphine (TBP) were purchased from Strem. $Cd(CH_3)_2$ was stored in a refrigerator in the drybox after being vacuum transferred. Selenium (Se), tri-*n*-octylphosphine oxide (TOPO), anhydrous methanol, anhydrous pyridine, and anhydrous toluene were purchased from Aldrich. Bis-trimethylsilane sulfide ($(TMS)_2S$) was purchased from Fluka.

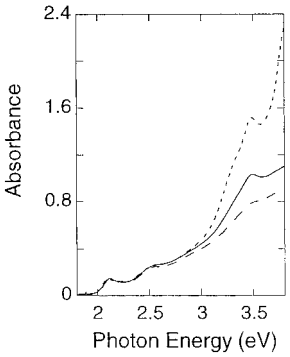

Figure 2. Absorption spectra of a core/shell and CdS-only nanocrystal mixture as synthesized (dashed) and after successive separations (solid and long dashed). The peak at 3.5 eV represents the CdS-only nanocrystals (see text), while the lower energy features are characteristic of the core/shell nanocrystals. During successive separations, the CdS-only peak intensity decreases relative to that of the core/shells, indicating successful separation.

Stock Solution for CdSe Nanocrystals Synthesis. The desired amount of $Cd(CH_3)_2$ was added to a solution of Se powder dissolved in TBP. Cadmium to selenium molar ratios were 1.0/0.7 or 1.0/0.9. The Se concentration was maintained near 0.20 mol/kg. Stock solutions were prepared in the drybox and stored under N_2 in the refrigerator.

Stock Solution for CdS Nanocrystal Synthesis. A solution of Cd $(CH_3)_2$ was dissolved in 3/1 TBP/toluene in the drybox. To this was added $(TMS)_2S$. The cadmium to sulfur molar ratio was 1.0/0.4. The sulfur concentration was maintained near 0.05 mol/kg.

Synthesis Procedure of CdSe and CdS Nanocrystals. For a typical synthesis, 12 g of TOPO was transferred to a three-necked flask and briefly heated to 360 °C under Ar flow on a Schlenk line. The stock solution (6 mL) was quickly (<1 s) injected into the hot TOPO using a large bore needle (17−12 gauge). The reaction was either stopped immediately by quickly removing the heating or allowed to continue after lowering the temperature to 300 °C for CdSe nanocrystals or 250 °C for CdS nanocrystals. Nanocrystal size was monitored by UV−vis spectra of aliquots taken from the reaction solution. The reaction was stopped by removing the heating after the desired size was achieved. This heating process can last from minutes to hours. Nanocrystals were precipitated by the addition of methanol to the cooled, room temperature reaction mixture. After centrifugation and drying under N_2 flow, a powder was obtained. Typically, hundreds of milligrams to a few grams of TOPO capped nanocrystals are synthesized by each reaction. No further size selective purification was done for the samples mentioned here. CdS nanocrystals of 35 Å diameter synthesized in this way were used in all experiments presented here, except those of Figure 2.

(B) Synthesis of CdSe/CdS Core/Shell Structure. Stock Solution for CdS Shell Growth. $(TMS)_2S$ (100 μL) was added to a solution of 0.033 g of $Cd(CH_3)_2$ dissolved in 3.81 g of TBP and stored under N_2 in refrigerator. The cadmium to sulfur ratio in this stock solution is 1.0/2.1. All the core/shell nanocrystals were synthesized using this stock solution except where noted.

(27) Halsall, M. P.; Nicholls, J. E.; Davies, J. J.; Wright, P. J.; Cockayne, B. *Surf. Sci.* **1990**, *228*, 41.
(28) Grun, M.; Hetterich, M.; Klingshirn, C.; Rosenauer, A.; Zweck, J.; Gebhardt, W. *J. Crystal Growth* **1994**, *138*, 150−154.
(29) Grun, M.; Hetterich, M.; Becker, U.; Giessen, H.; Klingshirn, C. *J. Crystal Growth* **1994**, *141*, 68.
(30) Murray, C. B.; Norris, D. J.; Bawendi, M. G. *J. Am. Chem. Soc.* **1993**, *115*, 8706.
(31) Bowen Katari, J. E.; Colvin, V. L.; Alivisatos, A. P. *J. Phys. Chem.* **1994**, *98*, 4109.

Procedure for Shell Growth onto CdSe Nanocrystals. TOPO (2−13 mg) capped CdSe nanocrystals were transferred to a three-necked flask, degassed, and purged with Ar on the Schlenk line. To this was added 15 mL of anhydrous pyridine. The nanocrystals dissolved readily, and the solution was allowed to reflux overnight under Ar flow. From 0.5 to 2 mL of diluted CdS stock (1:3 volume ratio of stock: TBP) was then added dropwise (1 drop per s) to the reaction solution at 100 °C. Absorption spectra of removed aliquots were recorded after each CdS addition.

Stopping the CdS addition and removing the heating completed the growth. Dodecylamine was added to the reaction solution at room temperature until the nanocrystals precipitated. Nanocrystals were isolated from solvents and unreacted reagents by centrifugation. These isolated, capped nanocrystals were readily soluble in $CHCl_3$ or CH_2Cl_2 but not pyridine.

(C) Characterization. UV−Vis Absorption Spectroscopy. Absorption spectra were obtained using an HP Model 8452 ultraviolet-visible absorption (UV−vis) diode array spectrometer with a collimated deuterium lamp source having a resolution of 2 nm. Samples were dispersed in toluene, chloroform, or pyridine for measurement.

Photoluminescence (PL) and Photoluminescence Excitation (PLE) Spectroscopy. Photoluminescence experiments were conducted on a Hitachi F-4500 fluorescence spectrometer with collection at 90° and resolution of 2.5 nm. Quantum yields of nanocrystal solutions were calculated by comparing the integrated emission to that of Rhodamine 6G or Rhodamine 640 in methanol. Optical densities of all solutions were below 0.3 at the excitation wavelengths used.

X-ray Diffraction (XRD). X-ray powder diffraction patterns were recorded using a Siemens Model D5000 X-ray diffraction with Cu Kα radiation. Nanocrystals were placed on quartz plates for measurement.

Transmission Electron Microscopy (TEM). Samples for TEM were deposited onto copper TEM grids coated with thin (5−50 nm thickness) carbon films. To improve adhesion of the nanocrystals to the carbon film, the grids were pretreated in an argon ion glow discharge (30 s in 50 mTorr argon). Immediately after the glow discharge a drop of nanocrystal dissolved in dimethyl chloride or chloroform was placed on a grid. The excess liquid was then wicked away with tissue, and the grid was allowed to dry in air. The grids were examined in a TopCon EM002B microscope with an Ultra-High Resolution (UHR) polepiece using a LaB_6 filament operated at 200 kV.

Nanocrystal sizes were measured by counting HRTEM fringe spacings directly off the micrograph negatives. The spacings used for size measurements were the *a* spacing (100 planes, 3.72 Å) and the *c* spacing (002 planes, 3.51 Å). These large spacings are easy to measure and not likely to be confused with other materials, such as oxides. When cross fringes are present in a nanocrystal, these two spacings can be uniquely identified based solely on the symmetry of the fringes observed. Even without full cross fringes, such spacings can frequently be identified by careful study of the detailed fringe contrast near the edges of the crystal, the location and orientation of stacking faults (which are parallel to 002 planes), and other considerations. For instance, as has been previously observed (see ref 30) and verified in this study, these nanocrystals are usually elongated along the *c*-axis. Hence simple fringes running perpendicular to the long axis are usually assigned to be (002) planes. Any misidentification of such planes will result in a systematic error in the measured nanocrystal diameter of at most $(|3.72-3.51|)/3.51 = 6\%$. This is considered to be an acceptable error as it allows the counting of many more nanocrystals to obtain good sizing statistics. In fact, this error is smaller than the statistical uncertainty in the measured diameters and is comparable to the discrepancy in describing prolate particles by a single average diameter. On the order of 150 nanocrystals were measured for each size distribution cited in this study.

Measurements of aspect ratio were undertaken only for nanocrystals exhibiting unambiguous cross-fringe contrast.

X-ray Photoelectron Spectroscopy (XPS). XPS was performed using a Perkin-Elmer PHI 5300 ESCA System. Thin cast films of nanocrystals were placed on evaporated gold films for measurement.

Results

Synthesis of Core/Shell Nanocrystals. Dropwise injection of CdS stock into a solution of CdSe nanocrystals as synthesized in TOPO and heated to 200 °C yields a product for which there was no evidence for the formation of a core/shell structure. It was then decided to attempt shell growth on a sample of CdSe nanocrystals precipitated and redissolved in a solvent more amenable to shell growth than TOPO. Pyridine was chosen as this solvent based on previous IR and XPS[31] experiments which revealed that, after refluxing in pyridine overnight, TOPO could almost completely be removed from CdSe nanocrystals without affecting the nanocrystal structure. Pyridine displaces TOPO and forms a weak bond to surface Cd atoms of CdSe nanocrystals. Furthermore, NMR studies have revealed that pyridine forms a labile bond to the surface Cd atoms when CdS nanocrystals are dissolved in pyridine.[32] Nanocrystals refluxed in pyridine are dynamically capped, providing simultaneous chemical stability and access to the surface. In addition to the use of pyridine, the reaction temperature was lowered to 100 °C, and the starting core (CdSe nanocrystal) concentration was lowered. This reaction is schematically shown in Figure 1.

Using these new conditions, and a Cd/S molar ratio in the stock of 1.0/0.7, the growth of a CdS shell was observed by UV−vis, PL, and TEM. However, the formation of CdS-only nanocrystals (having a first exciton peak in their absorption spectra near 3.4 eV (360 nm)) was also observed. CdS-only formation was also observed about 10 min after the injection of the same shell stock solution into pyridine (without cores) at 100 °C. These nanocrystals, suspected to be similar to $Cd_{32}S_{50}$ molecular species,[33] were found to be insoluble in pyridine, and for this reason could easily be separated from the core/shell nanocrystals. Figure 2 documents this separation for a somewhat anomalous sample in which a large amount of CdS-only nanocrystals were formed. As can be seen, each successive precipitation with methanol, centrifugation, and redissolution in methylene chloride removed a large percentage of the CdS while retaining the core/shell nanocrystals. These CdS nanocrystals were too small to have their crystal structure unambiguously determined using XRD.

By changing the Cd/S ratio in the stock solution to 1.0/2.1, the formation of CdS-only nanocrystals was prevented; only shell growth was observed. By checking the absorption spectrum of aliquots, it was found that shell growth was completed immediately after the addition of the stock solution.

The final achievable shell thickness was limited by the solubility of the core/shell nanocrystals; the reaction had to be stopped before the solution became turbid. This turbidity is thought to be the result of increased van der Waals interactions between nanocrystals brought about by their increased size, their dynamically capped surface, and the slightly polar nature of the solvent. The maximum achievable shell thickness depended on nanocrystal concentration, stock injection volume, and nanocrystal size.

Judicious control of the conditions for shell growth lead to quantitative use of the injected CdS stock solution. This is indicated both by the absence of a CdS-only peak in the absorption spectra and also by a quantitative correlation between the amount of injected stock and the average increase in nanocrystal size. This correlation was used to determine nanocrystal sizes in samples having very thin shells.

Absorption, Photoluminescence, and Quantum Yields. Plots of the photoluminescence (PL) and absorption spectra for two series of nanocrystals having two different core sizes and varying shell thicknesses are given in Figure 3. The core/shell nanocrystals were capped with dodecylamine and dissolved in methylene chloride. Unless otherwise stated, this capping group

(32) Sachleben, J. R.; Wooten, E. W.; Emsley, L.; Pines, A.; Colvin, V. L.; Alivisatos, A. P. *Chem. Phys. Lett.* **1992**, *198*, 431.

(33) Herron, H.; Calabrese, J. C.; Farneth, W. E.; Wang, Y. *Science* **1993**, *259*, 1426.

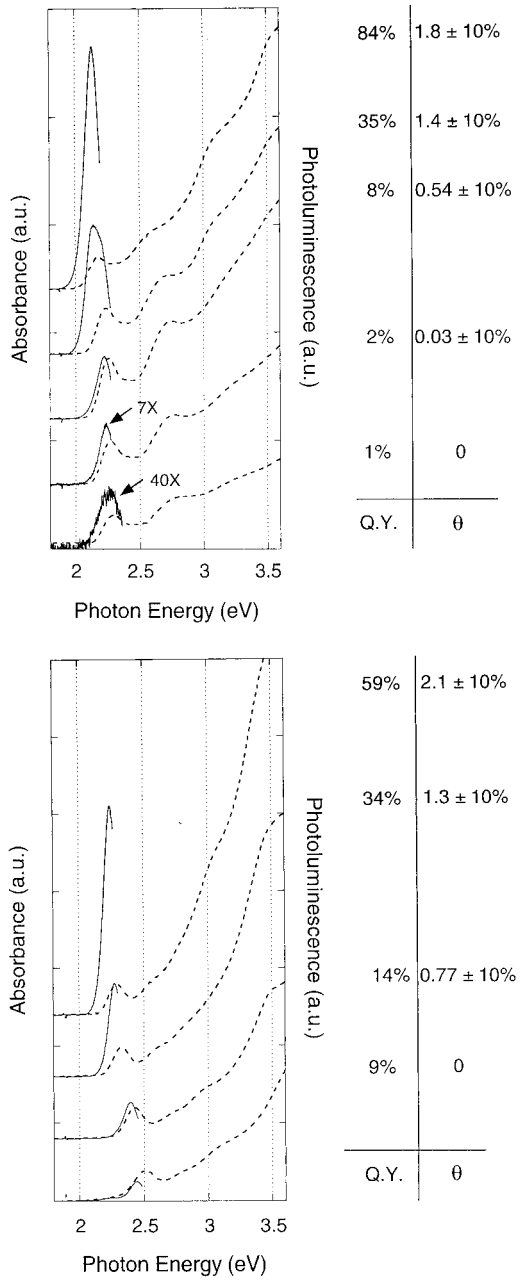

Figure 3. Absorption (dashed) and photoluminescence (solid) spectra of two series of core/shell nanocrystals. Spectra were taken after successive injections of CdS stock solution. The increase in quantum yield and of coverage of CdS with each injection is also shown. Q.Y.: quantum yield of photoluminescence. θ: number of monolayers of shell growth. All spectra were taken at a concentration corresponding to an optical density (OD) of roughly 0.2 at the peak of the lowest energy feature in the absorption spectrum. Figure 3A: 30 Å CdSe core diameter series; Figure 3B: 23 Å CdSe core diameter series.

was present on all samples. Throughout this paper, average sizes of core and core/shell nanocrystals (having thicker shells) were determined using HRTEM (see TEM section). Sizes of core/shell nanocrystals having shells thinner than approximately 3 Å were difficult to determine accurately using TEM. These sizes were determined based on the amount of injected CdS stock used in their synthesis. This sizing method was normalized to those sizes measured by TEM for thicker shell samples.

The core absorption spectrum is characteristic of nearly monodisperse nanocrystals with an absorption onset significantly shifted from the bulk value of wurtzite CdSe (1.74 eV). After refluxing the TOPO capped cores overnight in pyridine, no change was detected in their absorption spectra. These core

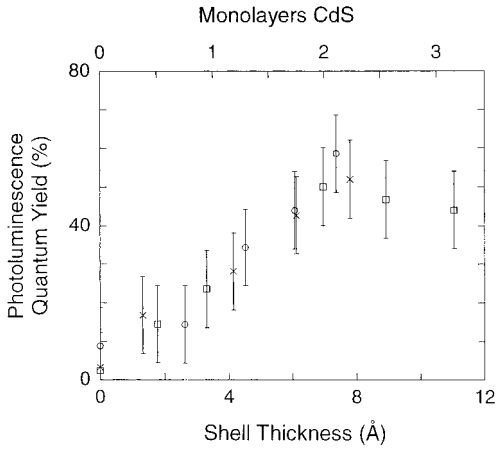

Figure 4. Photoluminescence quantum yield variation with shell thickness for three different core/shell syntheses starting with core diameters of 23 Å (circles), 34 Å (X's), and 39 Å (squares).

nanocrystals were capped with amine and used as a standard sample for comparison to core/shell samples in all experiments.

During shell growth, the absorption spectrum roughly maintained its overall shape, with a slight broadening of features, while shifting to lower energy. For the smaller cores a shift of approximately 0.05 eV accompanied each CdS stock injection, while smaller shifts of 0.02 eV per injection were observed for the larger cores. Smaller cores also showed a total absorption shift of near 0.17 eV, while larger cores showed a total shift of about 0.06 eV before the reaction mixture became turbid. These changes in the absorption spectra are caused by the closing together of electronic levels that accompanies a size increase[14] and by a slight worsening of the size distribution.

The PL spectra of Figure 3 result from excitation at or slightly blue of the first exciton peak in the absorption spectrum. The PL peaks reveal band edge luminescence for all shell thicknesses; no deep trap luminescence was detected. The shift of the peak of the PL from the first peak in the absorption spectrum is the result of a convolution of the size distribution and the emitting state.[34] This shift is also highly dependent on excitation energy for excitation near the first peak.[17]

Figure 4 shows the increase in quantum yield with shell thickness for three series of core/shell nanocrystals with cores of 23, 34, and 39 Å diameter. This increasing trend is observed up to a shell thickness of about three monolayers. (A shell thickness of ~3.5 Å corresponds to one full monolayer of growth.) The photoluminescence quantum yields (QY) increased from a few percent for core samples to at least 50% for samples with the thickest shells. It should be stressed that this 50% value is not an absolute limit. Samples have been synthesized with quantum yields near 100%. The core/shell nanocrystals of highest QY are seen to luminesce strongly under room lights.

PL, absorption spectra, and quantum yields were also collected for both core and core/shell nanocrystals lacking an organic capping group. For these, aliquots of nanocrystals in pyridine were removed from the reaction flask and immediately placed in a dark, air-free environment to eliminate oxidation of their bare surfaces. No dodecylamine was added. These air-free, uncapped nanocrystals showed absorption spectra unchanged from those having organic caps. The shape of their PL spectra, including their lack of deep trap luminescence and their trend of increasing intensity with shell thickness, was also similar to the capped nanocrystals. However, the quantum yields of these uncapped nanocrystals were between 15 and 20 times lower than their capped counterparts having identical core

(34) Nirmal, M.; Norris, D. J.; Kuno, M.; Bawendi, M. G. *Phys. Rev. Lett.* **1995**, *75*, 3728.

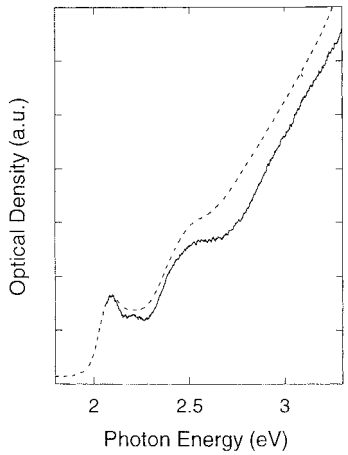

Figure 5. Photoluminescence excitation (solid) and absorption (dashed) spectra of a core/shell sample of 39 Å core diameter and 11 Å shell thickness. The PL was detected at 1.9 eV. The PLE spectrum closely tracks the absorption spectrum at all energies.

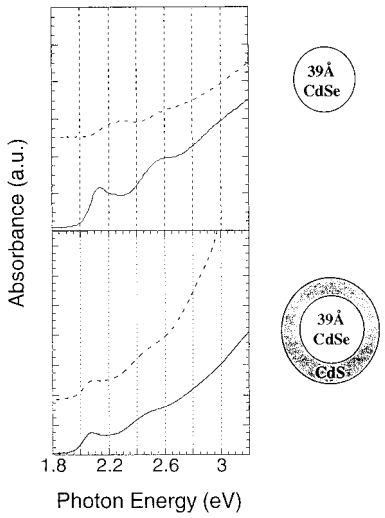

Figure 6. Photostability comparison of core and core/shell nanocrystals. Absorption spectra of core (top) and core/shell (bottom) samples before (solid) and after (dashed) continuous wave irradiation at 514 nm with an average power of 50 mW. The core is of 39 Å diameter, and the core/shell is made from this core with a 7 Å shell thickness. The solutions were saturated with oxygen and had identical optical densities at the excitation wavelength at the start of the experiment.

diameters and shell thicknesses. The uncapped core nanocrystals gave no detectable luminescence.

The PLE spectra of a very dilute (first exciton peak OD of 0.003, nanocrystal concentration of 1.4×10^{-8} M) solution of core/shell nanocrystals with a 39 Å diameter core and an 11 Å shell is given in Figure 5. The emission was detected at the peak of the sample photoluminescence (1.9 eV). At these low concentrations, the PLE spectrum closely tracks the absorption spectrum at all wavelengths of excitation. At higher concentrations, the PLE spectra diverged markedly from the absorption spectra at higher energies.[17]

Stability. Stabilities of core and core/shell nanocrystals were compared by a continuous wave laser photooxidation experiment. Figure 6 shows the results of an experiment on both core and core/shell sample of the same series. The core is of 39 Å diameter and the shell thickness is 7 Å. Both samples were dissolved in pyridine and lacked an organic capping molecule. The samples were saturated with oxygen throughout the experiment. The ODs of the two samples at the exciting wavelength (514 nm) were identical at the start. The laser power incident on each sample was 50 mW for approximately 2 h. A total of approximately 3×10^6 photons/nanocrystal were absorbed by the core/shell sample and about 50% less by the core sample because of its decreasing OD during the experiment.

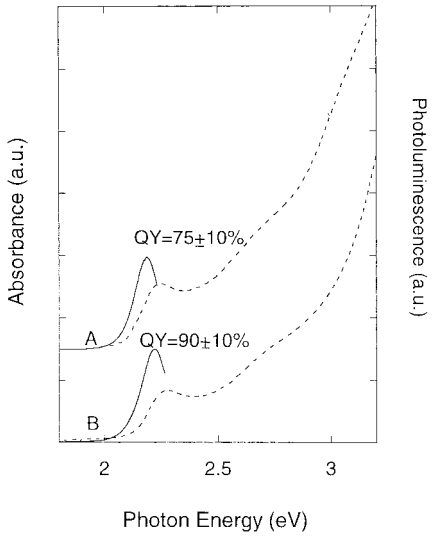

Figure 7. Quantum yield stability of core/shell nanocrystals. Photoluminescence (solid) and absorption (dashed) spectra of a core/shell sample of 27 Å diameter and 4 Å shell thickness before (a) and after (b) being left in air and room lights for 4 months.

The before and after absorption spectra of the two samples are in stark contrast. Relative to its absorption spectrum before irradiation, the core sample after irradiation showed a 0.16 eV (40 nm) shift of the first exciton peak to the blue, a general washing out of absorption features, and an overall decrease in OD throughout the energy range corresponding to nanocrystal absorption. This is a result of photooxidation of the nanocrystal.[15] In contrast, the core/shell absorption spectra showed little change after the photooxidation treatment. The first exciton peak showed no shift, and the overall OD and spectral shape were effectively unchanged.

A related photooxidation experiment was done on CdSe, CdS, and core/shell nanocrystals dissolved in chloroform saturated with oxygen. The core/shell sample had dodecylamine capping group, while the other two were capped with a mixture of dodecylamine and TOPO. The optical densities of the three samples were within 10% of each other below 375 nm. The CdS sample had an absorption peak at 418 nm, the CdSe at 582 nm, and the core/shell sample at 588 nm.

A 200 W xenon lamp illuminated the three samples simultaneously for 1 h at a large enough distance from the lamp to prevent significant heating. As above, the CdS and CdSe nanocrystals showed significant blue shifting (from 30 to 40 nm) of their absorption maximums and a general loss of optical density at all wavelengths of absorption. The core/shell spectrum showed neither, though this sample absorbed more photons than the others due to its higher optical densities at longer wavelengths. These qualitative results demonstrate the enhanced photostability of the core/shell nanocrystals as compared to the cores. Quantitative kinetic studies are of significant interest for the future.

The stability of core/shell quantum yields to air and room lights is shown in Figure 7. Absorption spectra and quantum yields were measured on a sample of core/shell nanocrystals capped with dodecyl amine before and after being left in air and room lights for 4 months. Little change in absorption spectra and an approximate 15% decrease in quantum yield were detected.

XRD. Figure 8 shows a series of core, core/shell, and CdS-only XRD patterns. The cores are 39 Å diameter, and the core/shell nanocrystals are grown from these. The CdSe core and

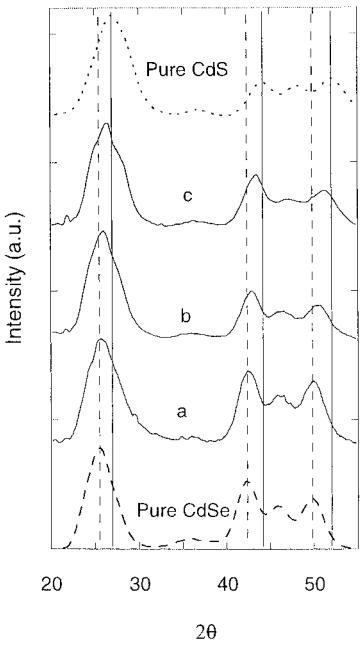

Figure 8. X-ray powder diffraction patterns of a pure CdS nanocrystal sample of 35 Å diameter (dotted), a CdSe core sample of 39 Å diameter (dashed), and core/shell samples having the same 39 Å core and shell thicknesses of (a) 2 Å, (b) 7 Å, and (c) 11 Å. The dashed vertical lines represent peak positions for pure CdSe; the solid lines represent pure CdS. A shift in core/shell peak positions from pure CdSe to pure CdS is observed upon shell growth.

CdS-only (high temperature TOPO synthesis; about 35 Å diameter) diffraction patterns exhibited peak positions corresponding to those of their bulk wurtzite crystal structures. The core/shell nanocrystal diffraction patterns were roughly the same shape (i.e., peak widths and relative peak intensities) as both the CdS-only and the CdSe core patterns. Upon shell growth, the entire spectrum systematically shifted in reflection angles from those characteristic of pure CdSe to those of pure CdS. For all samples, peak broadening due to finite size was observed at all reflections.

XPS. Figure 9 shows the results of XPS collected on three samples: 35 Å diameter CdS, 34 Å diameter CdSe, and core/shell nanocrystals having a 34 Å diameter core and a shell thickness of 18 Å. All samples were prepared air-free in identical manners, and for simplification in analysis, signal was collected over the same energy range for all samples.

The core/shell signal was fit (using commercial peak fitting software) with Gaussians representing the $S2p_{1/2}$, $S2p_{3/2}$, $Se3p_{1/2}$, and $Se3p_{3/2}$ peaks. For the fit, experimental values of the peak widths, intensity ratios between spin-orbit split states, and peak positions (as determined by the homogeneous nanocrystal signals) were used. Intensities were allowed to vary to obtain the best fit to the experiment. The atomic ratio of S/Se in the core/shell sample was determined to be 4.7/1 by dividing the integrated peak areas by the electronic core level sensitivity factors for each element. Note that the effect of the finite mean free path on the escape of photoelectrons from the core is significant (see Discussion).

TEM. Representative High Resolution TEM (HRTEM) micrographs of core and core/shell nanocrystals are presented in Figure 10. The fringe contrast reveals that the nanocrystals are in the wurtzite crystal structure. Additionally, the nanocrystals are somewhat faceted, consistent with previous observations on CdSe nanocrystals.[35] The average aspect ratio

(35) Shiang, J. J.; Kadavanich, A. V.; Grubbs, R. K.; Alivisatos, A. P. *J. Phys. Chem.* **1995**, *99*, 17417.

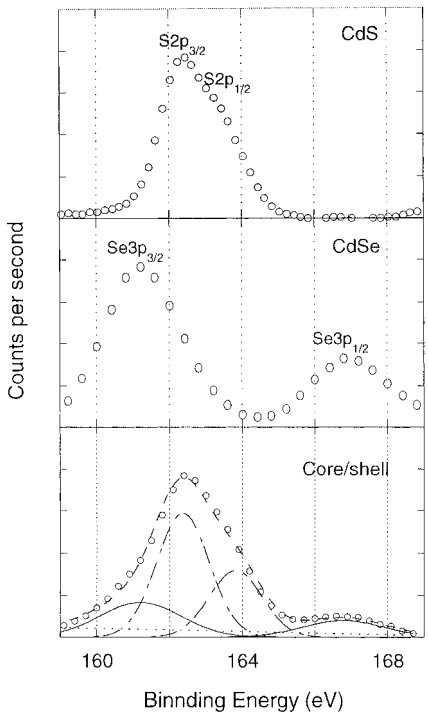

Figure 9. X-ray photoelectron spectra of thin cast films of pure CdS nanocrystals of 35 Å diameter (top), CdSe cores of 34 Å diameter (middle), and a core/shell sample of 34 Å diameter core and 9 Å shell thickness (bottom). The core/shell experimental data (circles) is fit by a Se3p contribution (solid), a S2p contribution (dashed/dot), and a linear background (dotted). The summed fit is given by the dashed line.

$$\left[A = \frac{\text{diameter}||c\text{-axis}}{\text{diameter}||a\text{-axis}}\right]$$

was 1.03 ± 0.015, and there was an average of 1.6 ± 0.2 stacking faults (rotation twin faults) per nanocrystal. The nanocrystals remained fully crystalline and somewhat faceted upon shell growth. There was no evidence for any defects at the core/shell interface. Indeed, the main indication of shell growth was the change in the nanocrystal diameter. In addition A increased to 1.10 ± 0.04, and the average stacking fault density increased to 2.2 ± 0.2 upon shell growth. All the observed stacking faults extended across the entire nanocrystal. This indicates that any stacking faults initially present in the core were preserved during shell growth and propagated through the shell, such as the example indicated by arrow 1 in Figure 10f. The increase in the stacking fault density is attributable to additional stacking faults occurring in the final layers of the shell structure, arrow 2 in Figure 10f. Nanocrystal sizing by TEM gave average core/shell size distributions of 10−15% over all samples. Size distributions were obtained by counting lattice fringes on a minimum of 150 nanocrystals. Core/shell size distributions were somewhat larger than those of the cores, consistent with the often observed broadening of the absorption spectra upon shell growth.

Evidence for the shell structure also arises from the image contrast. In HRTEM, contrast depends on the electron scattering power of the object forming the image. The electron scattering power in turn depends on the electron density inside the object. Hence, for similar lattice parameters CdS is expected to show less contrast than CdSe since it has fewer electrons per unit cell. This has been exploited previously to show elemental distributions in epitaxial nanocrystals.[24] In the present case, there was a noticeable drop-off in image contrast across the last 2−3 layers of the core/shell crystals in Figure 10f. To better visualize this change, intensity profiles along lattice planes in the images of Figure 10b,f and in a large CdSe nanocrystal

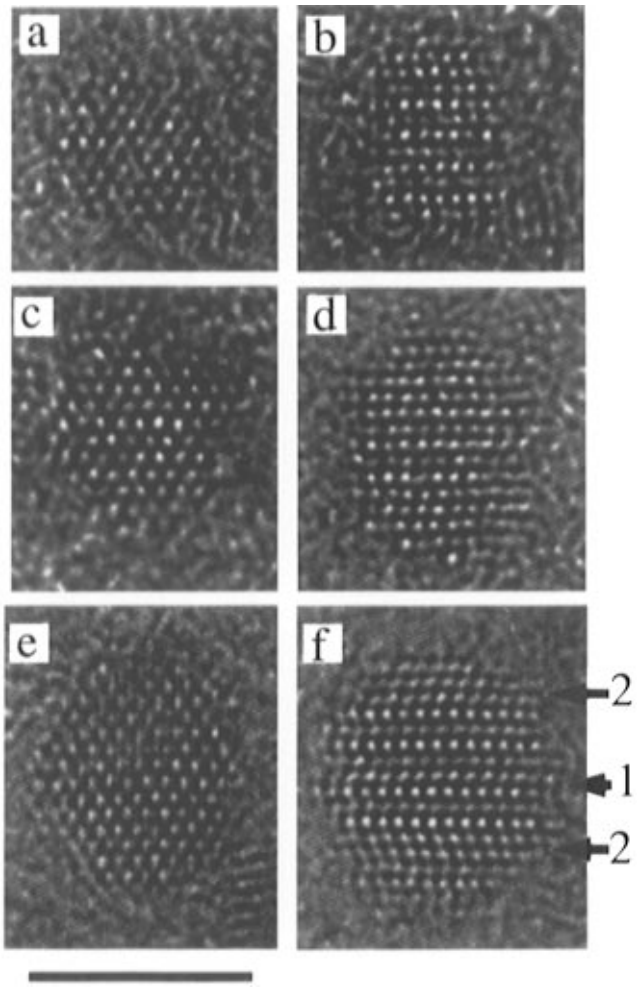

Figure 10. High resolution transmission electron micrographs (HR-TEMs) taken under black atom-contrast conditions near Scherzer defocus. Dark areas in the nanocrystal correspond to atomic positions, whereas bright spots indicate channels in the crystal structure. The length bar at the lower left corner indicates 50 Å. CdSe cores viewed along the (a) [001] zone axis (the wurtzite *c*-axis) and (b) [100] zone axis (with the *c*-axis in the image plane, pointing up). The random speckled background is due to the amorphous carbon substrate. In (a) faceting along (100) surface planes is evident, leading to a hexagonal shape in projection, which mimics the unit cell shape. The nanocrystal in (b) is faceted along (100) on the sides and (001) along the top/bottom. A rotation twin fault appears in the last layer along the top. The aspect ratio of this nanocrystal in this projection is 1.4. If a hexagonal shape is assumed, the *c*/*a* axis ratio is then 1.2. The poor contrast in images of such small nanocrystals is due to the background signal arising from the amorphous carbon substrate. (c) and (d) are core/shell nanocrystals with thin shells; (e) and (f) have thick shells. (c,d,e,f) are all grown from the cores shown in (a,b). (c) and (e) are shown in [001] projection, and (d) and (f) are shown in [100] projection. Similar faceting behavior is observed in (c,d,e,f). Arrow 1 in (d) marks a fault traversing the entire nanocrystal, including the core. Arrows labeled 2 indicate faults which traverse the nanocrystal but may or may not pass through the core. Additionally, there is a loss of contrast across the outer 2−3 layers, particularly noticeable along the left, top and bottom in (d). This suggests the presence of CdS in these layers, rather than the more strongly scattering CdSe.

(TEM not shown, line scan for comparison) were measured. Both the small cores and larger CdSe nanocrystals display a smooth drop-off in contrast near the edge of the nanocrystal, as shown in Figure 12a,c. By comparison, the core/shell nanocrystals exhibit a stepwise drop in contrast as seen in Figure 12b. This is consistent with a core/shell structure. A change in nanocrystal thickness may also explain such contrast, but it is unlikely that this would occur in such a steplike fashion, and this has never been observed in any other II−VI nanocrystal sample.

Figure 11 shows a full field view of core (a) and core/shell (b) nanocrystals. The cores have average diameter of 34 Å, and the core/shells are made from these cores and have a 9 Å shell thickness.

Discussion

I. Structural Characterization: Conditions for Shell Growth. The failure to grow CdS shells on the surface of CdSe cores as synthesized in TOPO at 200 °C is attributable to several factors. One explanation involves the presence of a growth-restricting TOPO layer on the surface of the cores, while another is the relatively high temperature. Other explanations are the rather high concentration of cores and the possible existence of some unreacted Cd and Se reagents still present in the mixture—both being requirements for a controlled core growth process. The high core concentration necessitates a high concentration of CdS stock for shell growth, and the reaction of this stock with the unreacted Cd and Se as well as homogeneous CdS nucleation would compete with shell growth.

The epitaxial growth of CdS on the surface of clean CdSe substrates (and vice versa) has been reported in the field of 2D superlattices.[13,27−29] Scaling this procedure to 3D growth in the nanocrystal regime presents several new challenges. The solution phase epitaxial growth of a CdS shell on the surface of CdSe cores is contingent on the suppression of homogenous CdS nucleation. While the rate of homogenous nucleation will increase with higher injected CdS concentration and higher temperature, the presence of an uncapped seed (the CdSe core) should promote shell growth. For these reasons, it was decided to attempt shell growth starting with redissolution of a core sample in pyridine, a solvent known to sustain a solution of dynamically capped CdSe nanocrystals.[31,32] The core concentration was decreased by a few orders of magnitude, and the shell growth temperature was set at 100 °C. This intermediate temperature was a compromise between the high temperature benefit of increased shell crystallinity and the low temperature benefit of suppressed homogeneous nucleation.

An explanation for why a lower Cd/S ratio promotes shell growth in pyridine is provided by the fact that the cores are synthesized using a cadmium rich stock solution. Therefore, they may have a cadmium rich surface, and the first layer of shell growth may be helped by a sulfur rich stock solution.

Shell Growth Does Not Form an Alloy. As detailed in the Results section, many of the characterization experiments support a model of core/shell growth rather than growth of a CdS_xSe_{1-x} alloy. Here, only the shift in the absorption onset (Figure 3) and the XPS results will be discussed in detail.

The prevention of alloying in CdS/CdSe heterostructures has been addressed previously in the area of 2D superlattice growth. Wurtzite CdS/CdSe superlattices with abrupt interfaces and periods of 45−800 Å have been grown by MOCVD with substrate temperatures of 450 °C.[13] Hot wall beam epitaxy, a growth technique perhaps more related to that presented here since it operates very close to thermodynamic equilibrium, has been used to grow similar defect free superlattices of 80 Å period with abrupt interfaces at substrate temperatures between 400 and 550 °C.[28] The significantly lower temperature of shell growth presented here must be considered along with the fact that nanocrystals have a much lower melting point compared to the bulk[36] and presumably a lower temperature for the onset of interatomic diffusion.

(36) Goldstein, A. N.; Echer, C. M.; Alivisatos, A. P. *Science* **1992**, *256*, 1425.

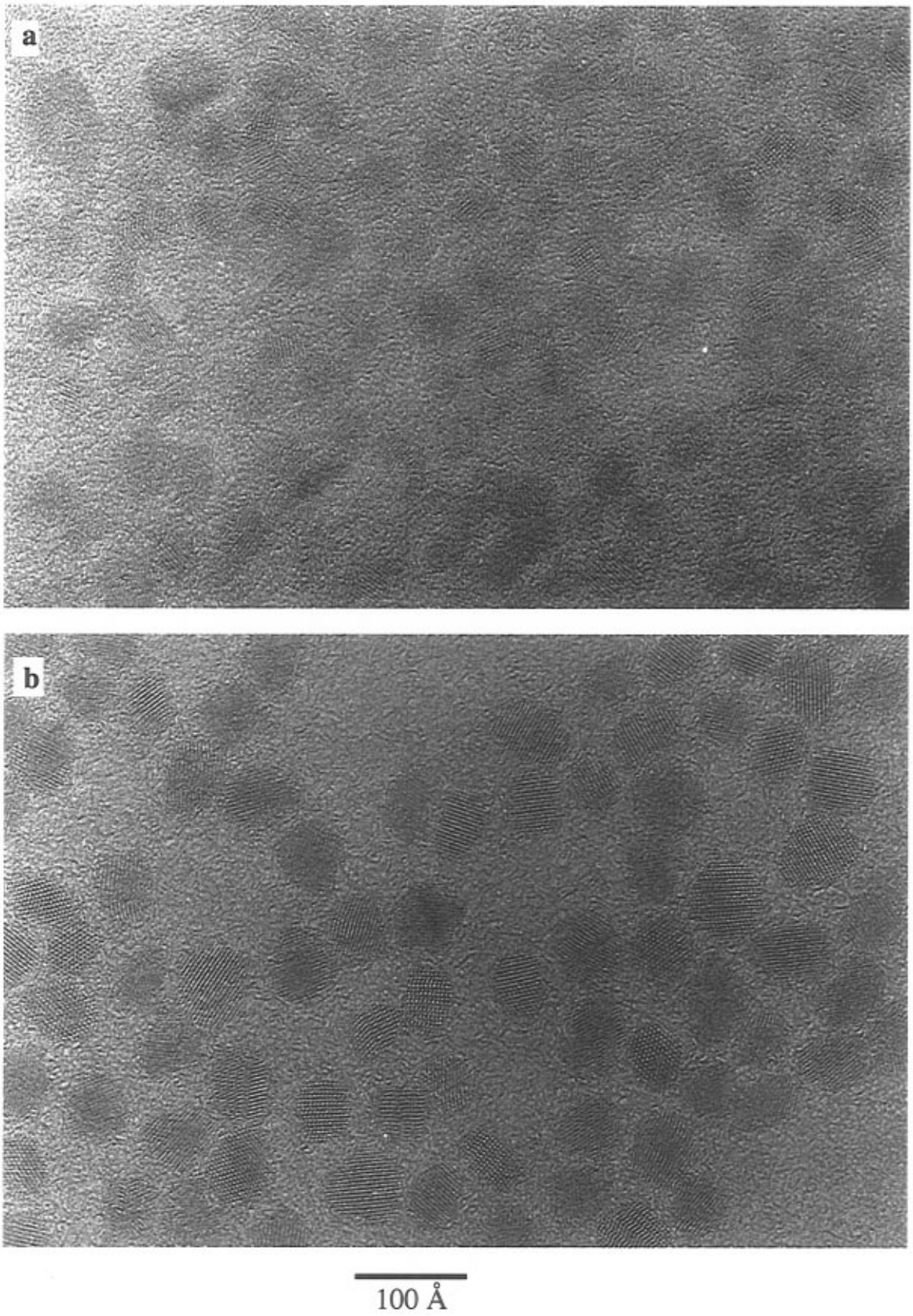

Figure 11. Wide-field HRTEMs of core (a) and core/shell (b) nanocrystals synthesized from these cores. The pictures are at the same magnification, indicated by the 100 Å length marker at the bottom. The core diameter is 34 Å and the shell thickness for the core/shell nanocrystals is 9 Å. The core/shell nanocrystals are clearly larger than the cores. Where lattice fringes are observed in the core/shells, they persist throughout the entire nanocrystal, indicating epitaxial growth. (The appearance of lattice fringes for a particular nanocrystal is a result of chance alignment.)

In the experiments presented here, the systematic *red* shift of the absorption spectra upon the incorporation of a larger band gap material (see Figure 3) is consistent with shell growth occurring without alloying. This point is best demonstrated by analogy. Alloys of composition CdS_xSe_{1-x} have bulk band gaps linearly related to molar content of chalcogenide by the

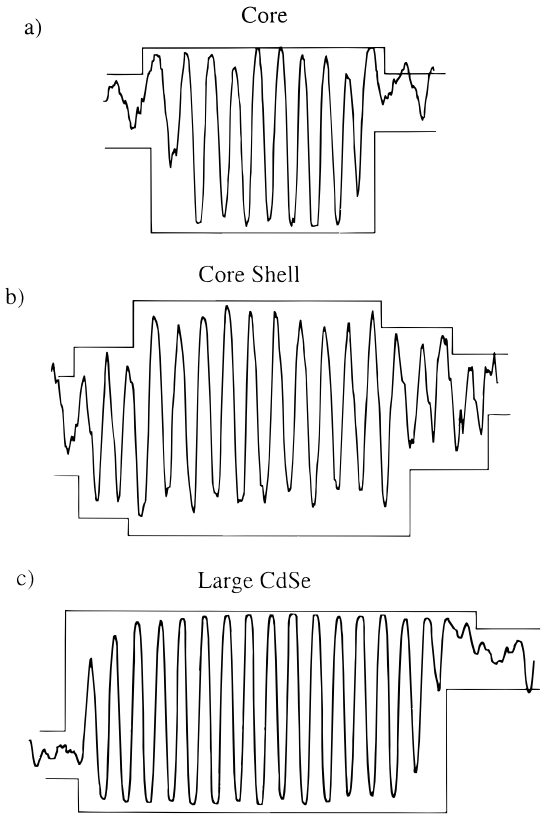

Figure 12. Horizontal intensity line profiles along lattice planes (taken from TEMs). Part (a) corresponds to Figure 10(b), 12(b) to 10(f), and 12(c) to a large CdSe nanocrystal of similar size to the core/shell nanocrystal shown in 10(f) (TEM not shown). All are on the same horizontal scale. Profiles are scaled vertically for maximum contrast. Peaks indicate atomic positions; valleys indicate channels. The boxed lines are guides to the eye to indicate a change in contrast level. For determining the edge of a nanocrystal, the peak spacing is also taken into account. While the cores (a,c) exhibit a smooth drop-off in contrast at the edges, the core/shell (b) loses contrast stepwise.

following equation[37]

$$E_g\,(\mathrm{nm}) = 718 - 210x$$

(718 nm is the bandgap of bulk CdSe and 210 nm is the bandgap difference between bulk CdSe (718 nm) and bulk CdS (508 nm)). Therefore, a bulk alloy having a 2.6/1.0 molar ratio of CdS/CdSe should have an absorption onset of 562 nm. Nanocrystal alloys having this molar ratio would show a first excitonic peak further blue of this value due to quantum confinement effects. However, a core/shell nanocrystal having this molar ratio was synthesized (34 Å average core diameter growing to 52 Å after CdS injection) with a first excitonic peak at 582 nm, far red of even the bulk alloy. This red shift upon shell growth was consistently detected, and is the result of a decrease of the kinetic energy of the excited electron and hole in the nanocrystal due to the spreading of their wave functions into the shell. Thus, considering absorption onsets alone, the possibility of alloying during shell growth can be discounted.

XPS provides further evidence for the core/shell structure and against alloying.[20] In XPS, the intensity of photoelectron signal originating from a given atom is given by

$$I = I_0 e^{(-z/\lambda)}$$

where I_0 is the unattenuated signal intensity, z is the distance of the emitting atom from the surface, and λ is the mean free path of the emitted electron (λ is both energy and material dependent). When the mean free path of the emitted photoelectron is comparable to shell thickness, XPS on thin films of core/shell nanocrystals can provide information about the thickness and uniformity of shell growth by comparing signal intensities from core and shell atoms.[20]

XPS signal was collected from the Se3p electronic core levels in core and core/shell nanocrystals and from the S2p levels in CdS only and core/shell nanocrystals (see Figure 9). Electrons originating from these two electronic core levels have very similar binding energies and nearly identical mean free paths (approximately 20 Å in the experiment presented here). In this case, integrated XPS peak areas can be used to determine molar ratios of S/Se by considering atomic core level cross-sections only.

The integrated areas gave an observed S/Se of 4.7/1 for the core/shell nanocrystals by only considering atomic core level cross-sections. From TEMs, the average diameter of the core and core/shell were determined to be 34 and 52 Å, respectively, giving a shell thickness of 9 Å and an actual S/Se of 2.6/1. The larger value of S/Se in the XPS signal is to be expected with a mean free path for all detected electrons of approximately two times the shell thickness. Electrons originating from Se atoms have a lower probability of escaping the nanocrystal and being detected. A simple calculation[31] using the integrated ratios from Figure 9, the known core radius, and assuming spherical nanocrystals with an abrupt interface gave a shell thickness of 12 Å in good agreement with the TEMs. The uniform shell thickness suggested by these results is consistent with the line scans (Figure 12) which reveal equally thick regions of CdS on either side of a CdSe core.

Shell Growth Yields a Crystalline Shell. Shell Growth Is Epitaxial. TEM combined with XRD provides the most substantial proof of a crystalline shell and epitaxial growth. TEMs revealed that, at all stages of shell growth, all nanocrystals (hundreds were examined in each case) were fully crystalline (see Figure 11). They showed clear lattice fringes and stacking faults extending completely across the nanocrystal. As exemplified in the HRTEMs of Figures 10 and 11, these observations indicate the high degree of extended structural order resulting from epitaxy.

Mews *et al.* reported the epitaxial growth of a CdS/HgS/CdS structure.[24] In that case, one monolayer of HgS was inserted between layers of CdS. HRTEM revealed that stacking faults at the interface can cause the growth of the CdS outer shell on the HgS monolayer to be out of registry with the CdS core. The shape of the resulting crystal was sometimes changed from a tetrahedral to a tetrahedral core with some outgrowths on the (111) surface. In this report, the persistence of shape and faceting in the core/shell nanocrystals is consistent with uniform shell growth in all directions and with epitaxy.

The core/shell XRD patterns are consistent with the model suggested by the TEMs of a wurtzite nanocrystal. Most notable in the XRD patterns shown in Figure 8 are the shift in peak positions toward CdS values and the constant peak widths at all stages of shell growth. These trends reveal no qualitative difference in structure between those nanocrystals having thin shells (less than a full monolayer) and those having thicker shells. Considering the shifts in peak positions alone, the XRD patterns could be indicative of alloying. However, a homogeneous alloy would show a significant narrowing of XRD peak widths with increasing size.

The lattice mismatch of 3.9% between the CdSe and CdS implies the possibility of strain existing between core and shell. In certain CdSe/CdS superlattices, strain has been shown to persist for up to 50 Å without relaxation.[28] Because nanocrystal

(37) Streckert, H. H.; Ellis, A. B. *J. Phys. Chem.* **1982**, *86*, 4921.

shell growth occurs in three dimensions, the strain in a nanocrystal should involve a larger volume fraction than in a superlattice and have a correspondingly larger effect on the XRD patterns. Consideration of lattice constants only would lead to the conclusion that the CdSe near the interface experiences a net compressive strain, while the CdS experiences a net expansive strain. Thus, there is expected to be a smooth increase in the average lattice constant and in the distribution of lattice constants throughout shell growth, even for submonolayer shell thicknesses. This is consistent with the observed peak shifts toward larger d-spacings. Indeed, the distribution of bond lengths resulting from strain is a possible explanation for why core/shell XRD peak widths stay about the same as those of the core despite the overall increase in nanocrystal size (see Figure 8).

Besides its obvious structural effects, strain could also affect the electronic properties of core/shell nanocrystals. However, strain could not cause the red shift of absorption spectra observed here with shell growth. Here, strain can only serve to decrease the lattice constant of the core (arising from the epitaxial growth of a material having a smaller lattice constant). This effect is known from high pressure experiments to shift the absorption spectra to the blue.[38] The extent to which strain persists in and how it affects the properties of these core/shell nanocrystals is still unclear, but the possibility of strain extending even throughout the entire structure cannot be eliminated. Modeling of the observed XRD patterns by a method previously outlined[30] is a future topic of research and could shed light on the degree to which strain affects the structure of these nanocrystals.

Figure 5 shows a high correlation of the PLE (of band edge emission) and the absorption spectrum of a highly diluted solution of core/shell nanocrystals. This is evidence for the efficient transfer of excitations of all energies to the core. This result is consistent with the removal of most of the core/shell interface defects (e.g., dangling bonds) to be expected from epitaxial growth and also with the growth of a defect free shell. With luminescence lifetimes known to be very long for homogeneous II-VI nanocrystals,[16,21] this efficient energy transfer between core and shell would seem to be a requirement for the high quantum yields observed and for the lack of any deep trap luminescence.

II. Electronic Structure: Photostability and Electronic Accessibility. Two important features of the structure and composition of these core/shell nanocrystals are electronic accessibility and photochemical stability. Both of these phenomena are a result of the details of charge confinement in these core/shell structures and are consistent with experimental observations.

The electronic levels of the core/shell nanocrystals are unique to this type of nanocrystal. Clearly, the core/shell optical properties do not reflect a superposition of CdS and CdSe electronic levels. They more reflect a perturbation of the core by a shell of large band gap material which serves to slightly decrease the confinement of and increase the quantum yield as compared to a core nanocrystal. This perturbation results in new electronic levels that extend throughout the entire structure. The conservation of shape but overall red shift of the absorption spectra of core/shell nanocrystals as compared to the core suggests this model.

It is possible to discuss the evolution of core/shell electronic levels from both a molecular and a particle-in-a-box viewpoint. They both result in a consistent model and correctly explain the experimentally observed electronic properties.

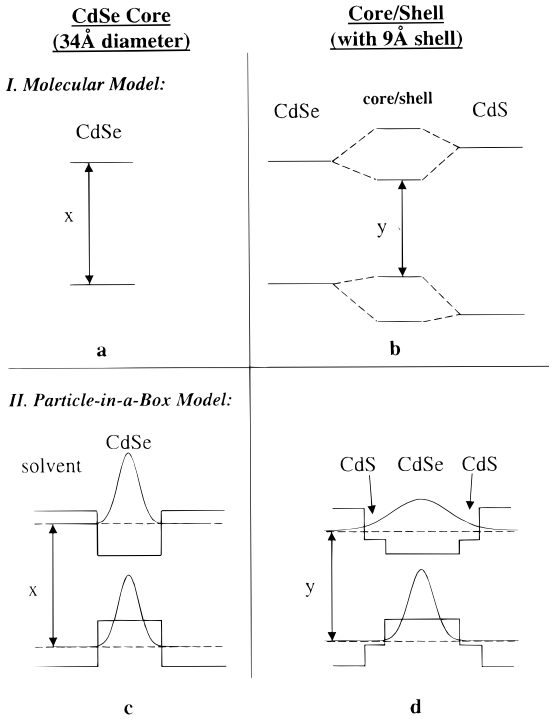

Figure 13. Schematic core and core/shell potentials (solid lines) and electronic energy levels (dashed lines) as described by a molecular model (a,b) and a particle-in-a-box model (c,d). (a,c) represent a core, while (b,d) represent a core/shell nanocrystal. "x" represents the absorption onset for a CdSe core of 34 Å diameter, "y" for a core/shell grown from this core with a 9 Å thick shell. The Gaussians shown are the results of effective mass calculations for electron and hole wave functions. From core to shell, the conduction band potential step is 0.27 eV, while that of the valence band is 0.51 eV. See text.

Molecular Orbital Model. The core/shell HOMO and LUMO energy levels can be qualitatively derived from a molecular orbital type framework (see Figure 13a,b). Here, the core and shell are viewed as molecular fragments. Because of a large quantum confinement effect, molecule-like discrete energy states are observed in CdSe-only and CdS-only nanocrystal absorption spectra.[8,9] In addition, since in core/shell nanocrystals the core and shell bond together epitaxially (thus conserving internal symmetry) and with minimal defects, their energy levels mix and a new set of core/shell levels emerge. The individual core and shell LUMOs will mix strongly since they are relatively close in energy (as determined by bulk electron affinities[39] and confinement theory applied to each part separately). Consequently, the core/shell LUMO will be largely delocalized throughout the structure. The energy difference between the core and shell HOMOs, however, is relatively large. The core/shell HOMO will be predominantly corelike in character and localized. Thus, electron/hole overlap in the core/shell first excited state is confined mostly to the core.

Particle-in-a-Box Model. The particle-in-a-box model can be used to obtain a first qualitative approximation of the electron and hole wave functions in the core/shell structure, providing insight into the extent of charge confinement. The parameters employed in this model must first be estimated. Figure 13 shows both the potentials (solid lines) and the overall electron and hole energy levels (dashed lines) along a line through the center of a core (c) and core/shell (d) nanocrystal. The core

(38) Tolbert, S. H.; Herhold, A. B.; Johnson, C. S.; Alivisatos, A. P. *Phys. Rev. Lett.* **1994**, *73*, 3266.

(39) Nethercot, A. H. *Phys. Rev. Lett.* **1974**, *33*, 1088.

(40) Schooss, D.; Mews, A.; Eychmuller, A.; Weller, H. *Phys. Rev. B* **1994**, *49*, 17072.

(41) Guzelian, A. A. *Synthesis and Characterization of III-V Semiconductor Nanocrystals*; Guzelian, A. A., Ed.; University of California: Berkeley, 1996.

diameter is 34 Å, and the core/shell has a shell thickness of 9 Å. Here, the potential offsets between the core and shell are approximated by the differences between the bulk electron affinities and ionization potentials of CdSe and CdS, as given by Nethercot.[39] This approximation yields a type I interface (i.e., an interface where there is a potential energy increase for both the hole and electron going from one material to the other). The electron (conduction band) potential step is about half as large as that of the hole (valence band) (0.27 vs 0.51 eV). It should be noted that the type of interface formed between two materials is very sensitive to the growth direction and possibly even the growth technique. (Cullis[13] and Klingshirn[12] have argued for a type II interface in their CdSe/CdS superlattices [grown by MOCVD and hot wall beam epitaxy, respectively].)

The electron and hole wave functions calculated with the particle-in-a-box model[40] are shown in Figure 13 (for wurtzite CdSe, $m_e = 0.12m_o$, $m_h = 0.45m_o$). These results suggest that the electron is delocalized throughout the core/shell structure, while the hole is mostly confined to the core. Further calculations (not shown in Figure 13) reveal an overall insensitivity of the electron and hole wave function extents to small changes in the energetic nature of the interface. That is, varying the conduction band potential offset between CdSe and CdS from +0.3 eV (type I structure) to −0.3 eV (type II structure) yields electron wave functions with significant density in both the core and shell and hole wave functions always localized predominantly in the core. Consequently, just as in the molecular orbital type picture, the electron/hole overlap in the first excited state is larger in the core than the shell. This is true, in the 34 Å diameter core case, even for shell thicknesses as large as 17 Å.

These results arise because the kinetic energy of the confined electron in this 0D structure is comparable to its potential step (kinetic energy being 0.35 eV with a potential step of 0.27 eV). For this reason, no clear distinction can be made between a type I and type II interface in these core/shell nanocrystals. This situation may occur frequently in 0D heterostructures where the kinetic energies of the charge carriers are comparable to their potential steps.

Interpretation of Experimental Results. These two models present a picture of core/shell energy levels that is consistent with many of the experimentally observed results.

The red shift in the absorption spectra upon shell growth seen in Figure 3 is predominantly a result of the high degree of mixing of the core and shell LUMOs in the molecular orbital model and the loss of quantum confinement in the particle-in-a-box model (a bigger box). The increased photostability of core/shell nanocrystals seen in Figure 6 is consistent with the confinement of the hole to the core. It has been shown experimentally that the main degradation mechanism in CdSe nanocrystals is photo-oxidation of surface selenium atoms to form selenium oxide.[31] This requires the presence at the nanocrystal surface of oxygen *and* a hole.[15] The increased stability argues that holes have a decreased probability of sampling the surface when a shell is present. Confinement of at least one of the charge carriers to the core would also be consistent with the very high observed quantum yields—as the highest probability of electron/hole overlap would then be in the core, away from the nonradiative traps and defects associated with the nanocrystal surface.

The spreading of the electron wave function into the shell that is predicted from the models is also consistent with experimental results. The delocalized excited electron wave function can sample the surface and be trapped by any uncapped surface cadmium atoms. The experimentally observed dependence of the quantum yield on the amine capping groups is understood since the capping group eliminates these traps for the delocalized electrons by binding to surface cadmium atoms. This is consistent with previous work on CdSe nanocrystals that concluded that electron donating organic capping groups form a donor/acceptor bond to surface cadmium atoms.[41]

This combination of photostability (hole confinement in the core), electronic accessibility (electron spreading into the shell), and high quantum yield makes these core/shell nanocrystals very attractive for use in optoelectronic devices like LEDs. In these applications, it is desirable to combine facile charge transport through a nanocrystal matrix with robust electroluminescent capability.

Acknowledgment. We thank K. Hamad for help with XPS calculations, N. Mizumoto for experimental assistance, and Dr. A. Mews for assistance with the wave function calculations. We also thank a reviewer for suggesting an experiment on the relative stability of CdS nanocrystals with respect to core/shell nanocrystals. NSF Grant DMR-9505302 provided financial support.

JA970754M